Instabilities of thermocapillary–buoyancy convection in open rectangular liquid layers*

Huan Jiang(姜欢)[1,2], Li Duan(段俐)[1,2,†], and Qi Kang(康琦)[1,2,‡]

[1] *Key Laboratory of Microgravity, Institute of Mechanics, Chinese Academy of Sciences, Beijing* 100190, *China*
[2] *School of Engineering Sciences, University of Chinese Academy of Sciences, Beijing* 100049, *China*

(Received 17 May 2017; revised manuscript received 7 July 2017; published online 30 September 2017)

This article presents the experimental investigation on instabilities of thermocapillary–buoyancy convection in the transition process in an open rectangular liquid layer subject to a horizontal temperature gradient. In the experimental run, an infrared thermal imaging system was constructed to observe and record the surface wave of the rectangular liquid layer. It was found that there are distinct convection longitudinal rolls in the flow field in the thermocapillary–buoyancy convection transition process. There are different wave characterizations for liquid layers with different thicknesses. For sufficiently thin layers, oblique hydrothermal waves are observed, which was predicted by the linear-stability analysis of Smith & Davis in 1983. For thicker layers, the surface flow is distinct and intensified, which is because the buoyancy convection plays a dominant role and bulk fluid flow from hot wall to cold wall in the free surface of liquid layers. In addition, the spatiotemporal evolution analysis has been carried out to conclude the rule of the temperature field destabilization in the transition process.

Keywords: thermocapillary–buoyancy convection, instability, open rectangular liquid layer, spatiotemporal evolution

PACS: 47.55.nb, 47.20.–k, 47.27.Cn, 44.10.+i **DOI:** 10.1088/1674-1056/26/11/114703

1. Introduction

Thermocapillary convection is driven by thermocapillary forces due to surface tension differences along the free surfaces of liquid layers. The coupling of thermocapillary forces with buoyancy forces is always present at normal gravity environment.[1] The investigation on thermocapillary–buoyancy convection instabilities is an age-long issue, especially on instabilities of surface waves. Smith and Davis[2,3] conducted a linear stability analysis on thermocapillary convection in an infinitely extended liquid layer subject to a horizontal temperature gradient. They predicted the propagation of oblique hydrothermal waves over the free surface. Parmentier *et al.*[4] also presented a linear stability analysis on buoyant-thermocapillary instabilities in a fluid layer of infinite horizontal extent, and explained the origin of longitudinal rolls. Priede and Gerbeth[5] studied the linear stability of thermocapillary–buoyancy convection in an extended liquid layer and explained the appearance of a steady multicellular flow, which ostensibly contradicts a "standard" linear theory predicting an oscillatory instability. Riley and Neitzel[6] experimentally observed and proved the existence of oblique hydrothermal waves in a rectangular liquid layer. They showed two different types of convection instabilities, including pure hydrothermal waves in sufficiently thin layers and steady multicell state and oscillatory state in thicker layers. Daviaud and Vince[7] reported experimental observations of traveling waves in a long and narrow container. The spatiotemporal properties of the traveling waves were studied in their paper. Burguete *et al.*[8] reported buoyant-thermocapillary instabilities in differentially heated liquid layers with different aspect ratios. They discussed the characteristics of oblique traveling waves and stationary longitudinal rolls, and compared two kinds of sources of waves. Ezersky *et al.*[9,10] researched experimentally the features of hydrothermal waves in rectangular and cylindrical containers through the method of shadowgraph. The spatiotemporal characteristics of the waves were studied by the Fourier transform. Some parameters of hydrothermal waves, including the frequency, the wavenumber, and the corresponding dispersion relation, could be concluded in their experiment. Garcimartín *et al.*[11] investigated experimentally the mechanism leading to instability in surface-tension-driven convection. Differential interferometry was used to observe the temperature field, and experiments indicated that a boundary layer instability led to the instability of surface waves. Pelacho and Burguete[12] reported an experimental study of a rectangular fluid layer on hydrothermal waves in thermocapillary–buoyancy convection. They observed a pair of oblique hydrothermal waves for certain values of the control parameters, and found that temperature oscil-

*Project supported by the Strategic Priority Research Program on Space Science, Chinese Academy of Sciences: SJ-10 Recoverable Scientific Experiment Satellite (Grant Nos. XDA04020405 and XDA04020202-05), the China Manned Space Engineering program (TG-2), Cooperative Research Project between China and Russia, and the National Natural Science Foundation of China (Grant No. 11372328).

†Corresponding author. E-mail: duanli@imech.ac.cn
‡Corresponding author. E-mail: kq@imech.ac.cn

© 2017 Chinese Physical Society and IOP Publishing Ltd

lations propagate in the direction of the temperature gradient. Schwabe *et al.*[13] investigated experimentally instabilities of shallow dynamic thermocapilllary liquid layers in an annular and a rectangular configuration. They observed different types of waves traveling in different thickness of liquid layers. Shevtsova *et al.*[14] investigated numerically thermocapillary–buoyancy convection in an extended cavity with differently heated walls. They predicted that when the Marangoni number *Ma* grows, the unicellular flow is replaced by a steady bicellular or multicellular flow and then either by a hydrothermal wave or an oscillatory multicellular flow, depending on the dynamic Bond number. Kang *et al.*[15] studied experimentally the surface deformation on buoyant–thermocapillary convection through an optical diagnostic system. The complicated relationships among temperature oscillation, velocity field, surface deformation and surface wave could be obtained in the experiment. Moreover, Duan *et al.*[16] also performed experimental study on liquid free surface in buoyant–thermocapillary convection. Surface deformations differ in various thickness liquid layers. Besides, Zhu *et al.*[17] investigated characteristics of surface oscillation in thermocapillary convection in a rectangular liquid container. They discussed the relationship of characteristics with the temperature difference and liquid layer depth. Zhou and Huang[18] researched numerically thermocapillary–buoyant convection in an annular two-layer system, and analyzed the flow pattern, the transition of flow pattern, and the interface deformability under various gravity levels.

In the present paper, different types of convection instabilities are observed and discussed in detail, and different types of convective instability patterns can be classified in rectangular liquid layers, which is the first comprehensive summary of our experimental model of the rectangular liquid layer. In addition, the spatiotemporal evolution analysis has been conducted to show the characteristics of surface waves, and one can understand the propagation of traveling waves more intuitively through this method.

2. Experimental setup and techniques

In order to investigate surface waves of rectangular liquid layers in an open rectangular container, we constructed an experimental system as shown in Fig. 1, which consists of a rectangular container, a temperature controller system, and an infrared thermal imaging system.

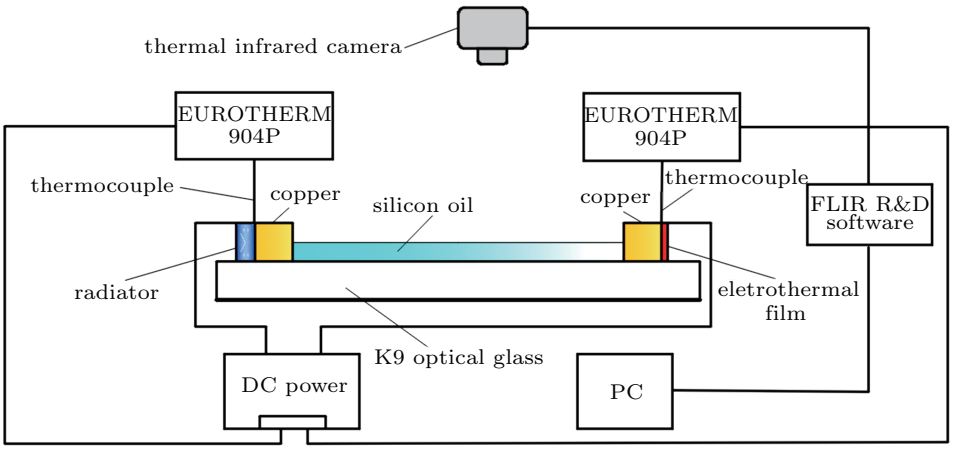


Fig. 1. (color online) The schematic diagram of the experimental system.

The rectangular container, shown in Fig. 2, is made of K9 optical glass with the thickness of 6 mm and two copper plates with the same thickness. The size of the rectangular container is 52 mm×108 mm×8 mm. The temperature controller system includes a semiconductor radiator used for lateral cooling, an electrothermal film used for lateral heating, a DC power, and two Eurotherm temperature controllers connected with T-type thermocouples. In our experiment, one copper wall was cooled by the semiconductor radiator while the other copper wall was heated by the electrothermal film. The Eurotherm temperature controllers could control the temperatures of the two copper walls by remotely controlling the DC power output. The precision temperature controlling is 0.1 °C.

The infrared thermography is a non-destructive measuring method which does not disturb the flow motion. This technique has been used to observe the dynamic characteristics of an evaporating drop in Refs. [19] and [20]. The thermal infrared camera is FLIR T420 with a thermal image resolution of 320 pixel×240 pixel and a thermal sensitivity of 0.05 °C. In our experimental run, the sampling frequency could be 15 frames per second (fps). The thermal infrared camera records images and video frequencies in the course of the experiment, which can be imported into the analysis software of FLIR R&D. In addition, an infrared macro lens was utilized to observe the local liquid layer. An observation region the size of 32 mm×24 mm could be chosen in the free surface of liquid

layers. This region is located in the middle of the free surface and kept a certain distance from the side wall, which could reduce the influence of the solid boundary.

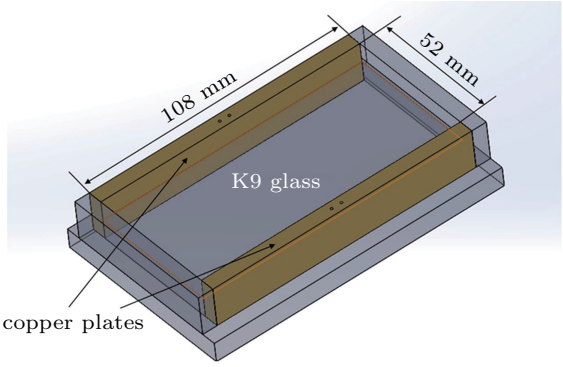


Fig. 2. (color online) The model figure of a rectangular liquid container.

The working fluid used in our experiments is Shin-Etsu KF96 silicone oil of 1 cSt, 1.5 cSt, and 2 cSt, which could be characterized by Prandtl number (Pr). Physical properties of silicone oil are listed in Table 1. In addition, we could control the influence of buoyancy by changing the thickness of the layer, which is defined as $\Gamma = L/d$. Here L is the length of the liquid layer between the cold-side and hot-side, and d is thickness of the liquid layer. The strength of thermocapillary convection is characterized by the Marangoni number, $Ma = \frac{(\partial\sigma/\partial T)(\Delta T/L)d^2}{\rho\nu\kappa}$, where ρ is the density, ν is the kinematic viscosity, κ is the thermal diffusivity, $\partial\sigma/\partial T$ is the temperature coefficient of surface tension, and ΔT is the temperature difference between the cold-side and hot-side. Besides, the dynamic Bond number could be introduced to measure the relative strength of the thermocapillary forces and buoyancy forces, $Bd = \frac{\rho g\beta d^2}{(\partial\sigma/\partial T)}$, where g is the gravitational acceleration, and β is the thermal-expansion coefficient.

Table 1. Physical properties of silicone oil.

Silicone oil (cSt)	Kinematic viscosity $\nu/10^{-6}$ m^2·s^{-1}	Density ρ/kg·m^{-3}	Thermal expansion coefficient $\beta/10^{-3}$ °C^{-1}	Thermal diffusivity $\kappa/10^{-8}$ m^2·s^{-1}	Surface tension $\sigma/10^{-2}$ N·m^{-1}	Temperature coefficient of surface tension $(\partial\sigma/\partial T)/10^{-5}$ N·m^{-1}·°C^{-1}	Pr
1	1	818	1.29	6.19	1.69	–7.55	16
1.5	1.5	852	1.27	5.95	1.77	–7.35	25
2	2	873	1.24	7.00	1.83	–7.16	29

In the course of our experiment, a linear temperature increase mode was adopted for an experimental period. The thermal infrared camera could record the thermal infrared image of surface waves, then we conducted further analysis on the thermocapillary–buoyancy convection instability.

3. Results and discussion

In our study, the thermal infrared camera was used to observe the temperature field of the liquid layer surface in the convection transition process. The convective instability includes three types of patterns: convection longitudinal rolls, traveling waves, and surface flow.

3.1. Convection longitudinal rolls

The first pattern is the appearance of convection longitudinal rolls. In the rectangular geometry, convection longitudinal rolls can be observed in thermocapillary convection when $\Gamma \geq 34.7$. The mode of convection longitudinal rolls shown in Fig. 3 differs in various layer thicknesses and is independent of Prandtl number. Figure 3 shows the convective structure by two types of visualization techniques. Figure 3(a) provides an overhead view of the temperature field visualized with the infrared thermography. The cross-section drawn of the velocity profile field by the method of PIV (the same method with Zhou *et al.*[21]) is shown in Fig. 3(b). This structure of rolls is generated by the gradient of surface tension in a liquid layer with a free surface. In general, convection longitudinal rolls widely exist throughout the whole process of convection transition and in various flow fields, including those of existences of traveling waves and surface flow.

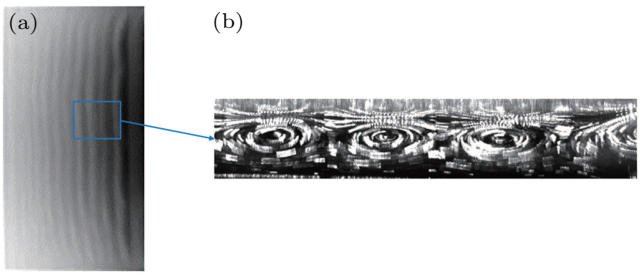


Fig. 3. The sketch map of convection longitudinal rolls: (a) the overhead view of the temperature field, (b) the cross-section drawn of the velocity profile field.

In the experiment, the wavenumber of convection longitudinal rolls differs in various aspect ratios. As shown in Fig. 4, selecting the same rectangular window for the constant Prandtl number and different aspect ratios of liquid layers, we could see different numbers of convection longitudinal rolls in the same window. Then the number of convection longitudinal rolls could be characterized by the nondimensionalized

wavenumber $\alpha = 2\pi d/\lambda$. As shown in Fig. 5, the wavenumber of convection longitudinal rolls shows a growing tendency with the aspect ratios of liquid layers, which signifies that there are different flow configurations for various thicknesses of the liquid layer. Besides, the flow field structure differs slightly in different Prandtl numbers.

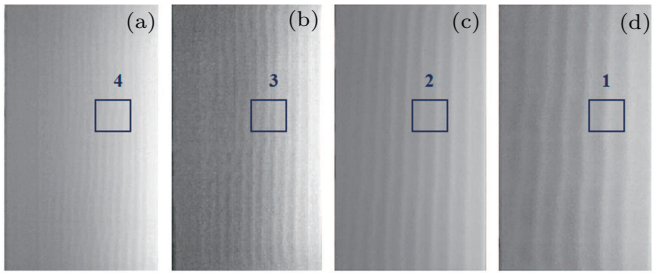


Fig. 4. The convection longitudinal rolls in different Γ and constant $Pr = 25$: (a) $\Gamma = 28.9$; (b) $\Gamma = 26$; (c) $\Gamma = 21.7$; (d) $\Gamma = 18.6$. The cold side is left.

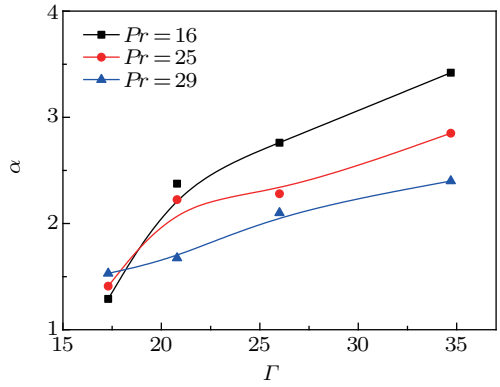


Fig. 5. (color online) The variation of wavenumber α of the convection longitudinal roll with aspect ratio Γ of the liquid layer.

In addition, convection longitudinal rolls oscillate back and forth with the increase of the temperature difference (the Marangoni number, similarly hereinafter). When the sufficient temperature difference is reached in the convection, the structure of convective rolls is broken by surface fluctuations, and the convection transits to oscillatory convection. This convective structure is similar to the steady multicellular flow in a thin rectangular geometry observed by Riley.[6]

3.2. Traveling waves

In this paper, traveling waves refer to hydrothermal waves, which propagate obliquely from the cold wall to the hot wall. In these experimental conditions, that is $Bd < 1$, thermocapillary convection is the dominating convection pattern.

When $Bd < 1$ and $20.8 \leq \Gamma \leq 34.7$, the distinct traveling wave could be observed. Two sets of representative experiments were selected here. Figure 6 shows the traveling wave in experimental conditions of $\Gamma = 34.7$ and $Pr = 16$. As shown in Fig. 6(a), the thermocapillary flow only presents convection longitudinal rolls with the small Marangoni number ($Ma = 871$), which is the two-dimensional flow. When the Marangoni number increases to a threshold ($Ma = 1574$), the flow destabilizes into a three-dimensional flow and traveling waves appear riding on top of convection longitudinal rolls, as shown in Fig. 6(b). Hydrothermal waves propagating obliquely from the cold wall to the hot wall were predicted by Smith and Davis.[2,3] In our experiments, the propagation characteristics of hydrothermal waves are in perfect accordance with Smith and Davis' prediction, also just as the experimental results of Riley.[6] The appearance of hydrothermal waves is because the structure of convective rolls fails to cope with heat transport requirements. When the Marangoni number is large enough ($Ma = 1807$), shown in Fig. 6(c), hydrothermal wave superposition and oscillatory convection appear in the free surface of liquid layers. Subsequently, surface traveling waves become irregular and confused with further increasing Ma.

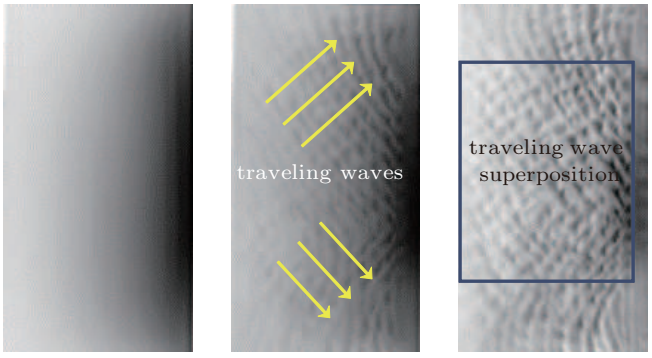
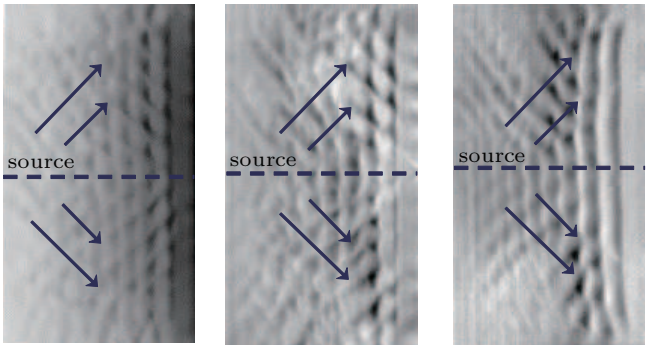


Fig. 6. (color online) Hydrothermal waves in the free surface of liquid layers in the experimental condition of $\Gamma = 34.7$ and $Pr = 16$. The Marangoni number increases gradually from panel (a) to panel (c). The cold side is left.

The location of the source of the traveling waves could be investigated in experimental conditions of Γ = 26 and different Pr (Fig. 7). From Fig. 7(a) to Fig. 7(c), we can all observe the oblique traveling wave similar to that in Fig. 6(b). Because the boundary layer around the liquid layer is uniform and symmetrical, the isotherm presents the characteristic of symmetric distribution depending on the experimental configuration. In consequence, there are two trains of symmetrical waves intersecting and overlapping obliquely in the free surface, and the symmetry axis is exactly the origin of the waves. The source is a line, generating two trains of waves from one end to the other end of the container. Hydrothermal waves transport heat in a sustained and steady manner, thereby the convective system could remain constant. This state of regular traveling waves lasts for a period of time, and then the oscillatory flow appears along with the hydrothermal waves when the Marangoni number is large enough.

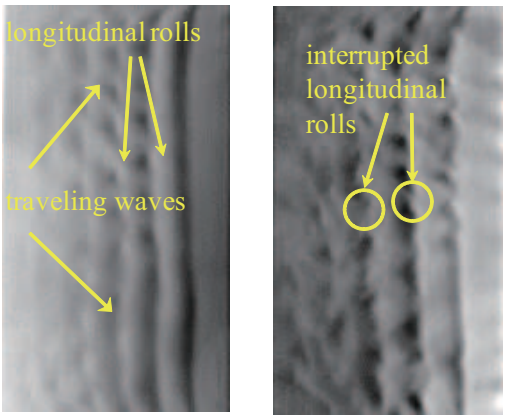
Actually, there exists the interplay of hydrothermal waves and convection longitudinal rolls in the process of convection

transition, which is obvious and distinct in Fig. 8. In the experimental condition of $\Gamma = 20.8$ and $Pr = 25$, as shown in Fig. 8(a), the traveling waves superimpose on the structure of convection longitudinal rolls, which constitutes the convective instability when $Ma = 2475$. When $Ma = 3079$, as shown in Fig. 8(b), intense surface fluctuation and oscillatory convection have interrupted the structure of rolls and cause numerous defects of longitudinal rolls, which also further intensifies the convective instability. The nonlinear interaction of various surface fluctuation results in the surface oscillation and instability, which is the thermocapillary dominated type-I oscillatory flow. In this experiment condition, it is noted that some weak surface disturbances originating from the thermal boundary layer and caused by buoyancy effects arise superimposed on the traveling waves when *Bd* is approximately equal to 1.



(a) $Ma = 1812$ (b) $Ma = 1963$ (c) $Ma = 1586$

Fig. 7. The source of hydrothermal waves in the free surface of liquid layers in constant $\Gamma = 26$ and various Pr: (a) $Pr = 16$; (b) $Pr = 25$; (c) $Pr = 29$. The cold side is left.



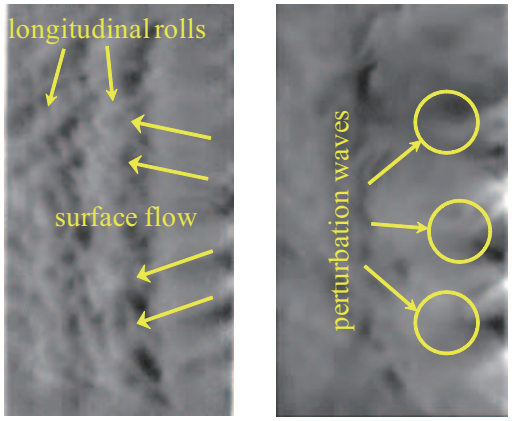
(a) $Ma = 2475$ (b) $Ma = 3079$

Fig. 8. (color online) Hydrothermal waves and convection longitudinal rolls in the free surface of liquid layers in the experimental condition of $\Gamma = 20.8$ and $Pr = 25$. The cold side is left.

3.3. Surface flow and perturbation waves

In our experiment, we also observed the surface flow, which originates from the unstable thermal boundary layer and results from effects of buoyancy convection.

When $\Gamma \leq 20.8$, namely, $Bd \geq 1$ (in Fig. 9), buoyancy effects dominate the convection and surface flow of bulk fluid appears in the free surface of liquid layers, which is the instability of buoyancy convection. In the buoyancy dominated flow, as shown in Fig. 9(a), the bulk fluid flow riding on top of convection longitudinal rolls from the hot side to the cold side could be presented, and this flow has been intensified with the increase of the Marangoni number. Indeed, a surface flow comes into being because the fluid at the bottom of the thermal boundary layer expands with heat, then the thermal fluid ascends quickly in the bottom and generates the surface flow from the hot side to the cold side in the free surface.



(a) $Ma = 4333$ (b) $Ma = 7662$

Fig. 9. (color online) Surface flow and perturbation waves in the free surface of liquid layers in different experimental conditions: (a) $\Gamma = 17.3$, $Pr = 25$; (b) $\Gamma = 14.9$, $Pr = 16$. The cold side is left.

In fact, an unstable thermal boundary layer could also result in the appearance of perturbation waves, as shown in Fig. 9(b). Perturbation waves begin to appear in the free surface when the Marangoni number is large enough. On account of a boundary layer instability near the hot wall, small perturbations inside the boundary layer are dragged and amplified downflow. This type of wave is analogous to waves observed by Garcimartín.[11] When the Marangoni number is large enough, intense buoyancy effects expand to the whole flow field and significant oscillatory flow arises. The overlap and interplay of surface flow and various perturbation waves constitute the buoyancy dominated type-II oscillatory flow. In principle, in this experimental condition, hydrothermal waves still exist in the free surface, but are covered up by the instability of buoyancy convection.

3.4. Stability diagram of thermocapillary–buoyancy convection

The flow can destabilize into different patterns, depending on the two parameters Ma and Γ. Therefore, the stability diagram of Fig. 10 shows a dependence of the threshold values on Ma_c (the critical Marangoni number) and Γ (aspect ratios). In every experimental period, the convection destabilizes to different patterns with the increase of the Marangoni

number. When the Marangoni number is small, the convection is a two-dimensional flow in the region named steady flow (SF); moreover, the flow transits to a three-dimensional flow in the region named hydrothermal waves (HTW) or surface flow (SUF), as the Marangoni number increases; finally, the three-dimensional flow starts to oscillate in the region of type-I oscillatory flow (TYPE-I OF) or type-II oscillatory flow (TYPE-II OF) when the Marangoni number is large enough. In addition, vertical dashed lines, that is $Bd = 1$, distinguish surface fluctuations into HTW and SW in the middle region of the three-dimensional flow. As is shown from Fig. 10(a) to Fig. 10(c), there are similar flowing characteristics for various Prandtl numbers, but only the critical Marangoni number differs in different Prandtl numbers.

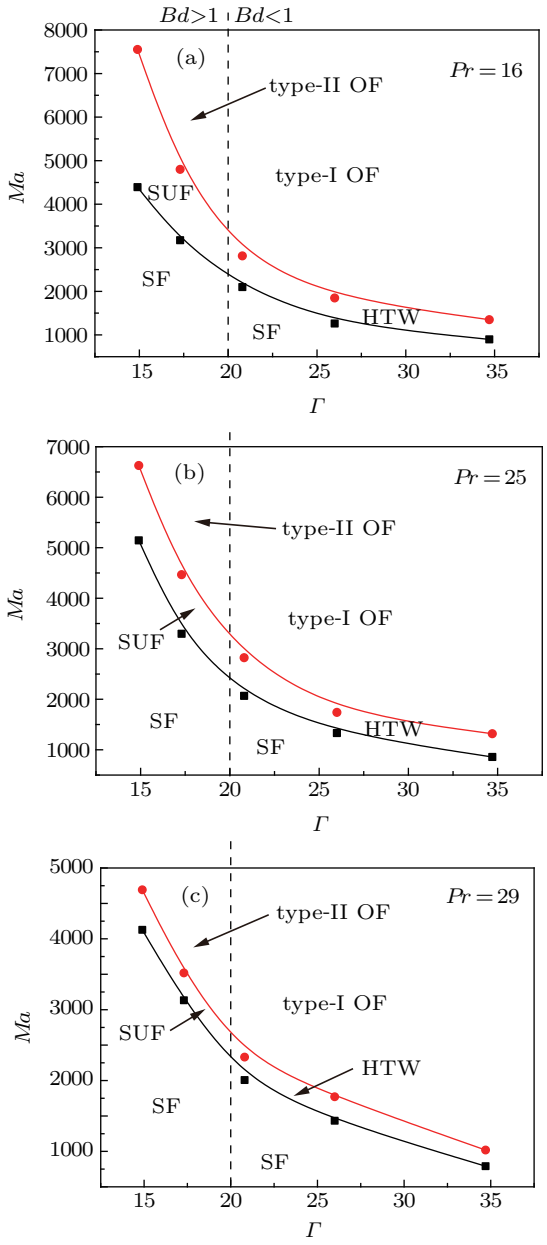


Fig. 10. (color online) Stability diagram: the critical Marangoni number Ma_c (solid lines with closed symbols) vs. aspect ratios Γ of the liquid layer for (a) $Pr = 16$, (b) $Pr = 25$, (c) $Pr = 29$. Vertical dashed lines correspond to the dynamic Bond number Bd.

3.5. The spatiotemporal evolution analysis

The rule of surface fluctuation could be concluded through the spatiotemporal evolution analysis. As shown in Fig. 11, the vertical line y and the horizontal line x are selected respectively from the free surface, and then spatiotemporal evolution diagrams can be drawn in different Marangoni numbers. In the spatiotemporal evolution diagrams of Figs. 11(a) and 11(b), every time range of gray bar denotes a course of spatiotemporal evolution in the same Marangoni number, and the Marangoni number increases gradually from top to bottom or from left to right. Take the experiment of $\Gamma = 26$ and $Pr = 25$ for example. The properties of wave propagations and oscillations over time in a line across a free surface could be drawn clearly in Fig. 11. As we can see, with the increase of the Marangoni number, it goes through three stages in the convection: no wave, regular traveling waves, traveling waves along with oscillatory convection.

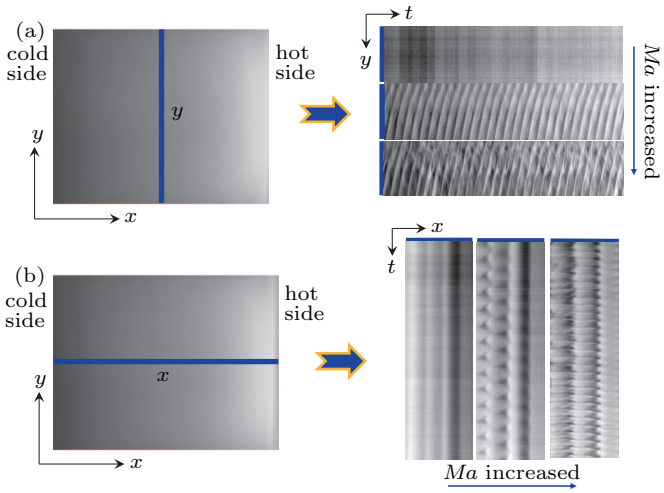


Fig. 11. (color online) The platform of the selected line in the free surface and spatiotemporal diagrams of infrared imageries in different directions: (a) y direction, (b)x direction.

Two sets of courses of spatiotemporal evolution in different experimental conditions have been enumerated in Figs. 12 and 13. Spatiotemporal evolution characteristics can be analyzed combining the line y with the line x. As shown in Figs. 12(a) and 12(b), when $\Gamma = 26$ and $Pr = 25$, there is no wave in the free surface at the small Marangoni number; then regular traveling waves appear in the gray bar when the Marangoni number increases to a threshold; traveling waves with oscillations eventually come into being at a large Marangoni number. In addition, we can also observe the convection longitudinal roll ridden on by regular traveling waves in Fig. 12(b). Likewise, when $\Gamma = 17.3$ and $Pr = 25$, as shown in Figs. 13(a) and 13(b), there is a comparable traveling wave in the transition process. In this experimental condition, buoyancy effects dominate the convection, and surface flow of bulk fluid appears along with the traveling wave in the free surface.

Similarly, it goes through no fluctuation, regular fluctuations, and fluctuations with oscillations in the process of transition with the increase of the Marangoni number in the convection.

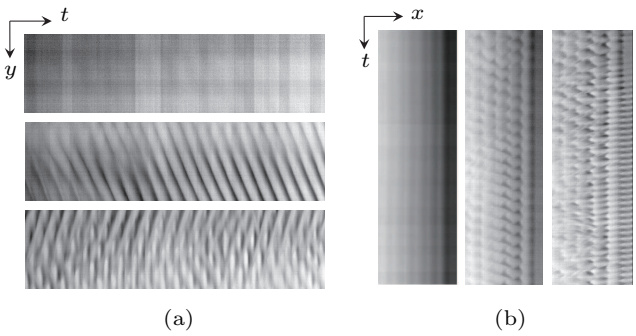


Fig. 12. Spatiotemporal evolution diagrams in the experimental condition of $\Gamma = 26$ and $Pr = 25$: (a) spatiotemporal evolution of the line y, (b) spatiotemporal evolution of the line x.

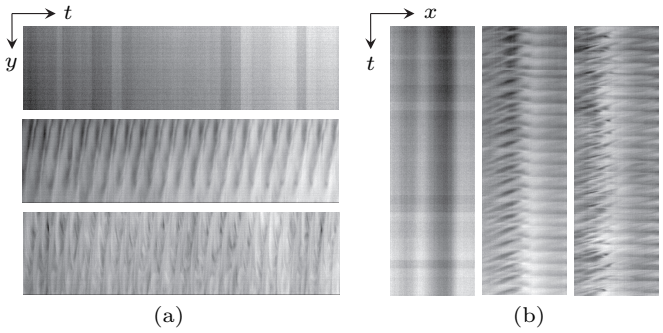


Fig. 13. Spatiotemporal evolution diagrams in the experimental condition of $\Gamma = 17.3$ and $Pr = 25$: (a) spatiotemporal evolution of the line y, (b) spatiotemporal evolution of the line x.

Table 2. The wave velocity and wave propagation angle of hydrothermal waves in various experimental conditions.

Experimental conditions	V/mm·s^{-1}	$\Theta/(^\circ)$
$Pr = 16, \Gamma$ =34.7	4.2	56.7
$Pr = 16, \Gamma = 26$	5.0	48.3
$Pr = 25, \Gamma = 34.7$	4.3	51.5
$Pr = 25, \Gamma = 26$	4.9	47.5
$Pr = 29, \Gamma = 34.7$	4.1	53.5
$Pr = 29, \Gamma = 26$	5.0	49.4

Furthermore, characterizations of hydrothermal waves' propagation, including the wave velocity and wave propagation angle, have been investigated by maps of spatiotemporal evolution. Through the spatiotemporal diagrams of infrared imageries in x and y directions, the propagation speed of traveling waves could be quantified. As shown in Fig. 14, the two wave velocity components V_x and V_y could be calculated, and then the resultant velocity V and the propagation angle Θ of hydrothermal waves could also be figured out by this means.

As listed in Table 2, there is little difference in the magnitude of velocity under the same Γ and in various Prandtl numbers. Also, the wave velocity and the wave propagation angle are more dependent on the variation of Γ to some extent.

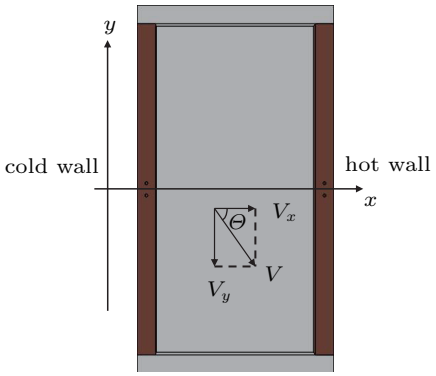


Fig. 14. The schematic plan for wave velocity and propagation angle of hydrothermal waves.

4. Conclusions

In the present paper, detailed observations and analyses on thermocapillary–buoyancy convection instabilities in open rectangular liquid layers have been conducted by using a thermal infrared camera. In particular, we adopted innovative infrared observation methods with a macro lens and performed spatiotemporal evolution analysis originally on infrared imagery of surface fluctuations. Besides, it is a distinctive and original research with an overall summarization and special distinction on various types of instabilities of thermocapillary–buoyancy in rectangular liquid layers.

In the experiment, convection longitudinal rolls have always existed throughout the process of convection transition. Traveling waves appear in the free surface of liquid layers when $Bd < 1$, and surface flow and perturbation waves appear in the flow field when $Bd \geq 1$. The spatiotemporal evolution analysis could be performed to demonstrate wave characteristics in the transition process of convection. The wave velocity and wave propagation angle of traveling waves can be measured in spatiotemporal diagrams of respective experimental conditions. The characterization of hydrothermal wave propagation is more dependent on the variation of Γ due to different flow field structures. Different types of convective instabilities are dependent on different flow field structures, which has generally been influenced by buoyancy effects in a normal gravity environment.

References

[1] Bach C and Schwabea D 2015 *Eur. Phys. J. Special Topics* **224** 319
[2] Smith M K and Davis S H 1983 *J. Fluid Mech.* **132** 119
[3] Smith M K and Davis S H 1983 *J. Fluid Mech.* **132** 145
[4] Parmentier P M, Regnier V C and Lebon G 1993 *Int. J. Heat Mass Transfer* **36** 2417
[5] Priede J and Gunter G 1997 *Phys. Rev. E* **56** 4187
[6] Riley R J and Neitzel G P 1998 *J. Fluid Mech.* **359** 143
[7] Daviaud F and Vince J M 1993 *Phys. Rev. E* **48** 4432
[8] Burguete J, Mukolobwiez N, Daviaud F, Garnier N and Chiffaudel A 2001 *Phys. Fluid* **13** 2773
[9] Ezersky A B, Garcimartín A, Mancini H L and Pérez-García C 1993 *Phys. Rev. E* **48** 4414
[10] Ezersky A B, Garcimartín A, Mancini H L and Pérez-García C 1993 *Phys. Rev. E* **47** 1126

[11] Garcimartín A, Mukolobwiez N and Daviaud F 1997 *Phys. Rev. E* **56** 1699
[12] Pelacho M A and Burguete J 1999 *Phys. Rev. E* **59** 835
[13] Schwabe D, Möller U, Schneider J and Scharmann A 1992 *Phys. Fluids A* **4** 2368
[14] Shevtsova V M, Nepomnyashchy A A, and Legros J C 2003 *Phys. Rev. E* **67** 066308
[15] Kang Q, Duan L and Hu W R 2004 *Microgravity Sci. Technol* **15** 18
[16] Duan L, Kang Q and Hu W R 2008 *Chin. Phys. Lett.* **25** 1347
[17] Zhu P, Zhou B, Duan L and Kang Q 2011 *Exp. Therm. Fluid Sci.* **35** 1444
[18] Zhou X M and Huang H L 2012 *Chin. Phys. Lett.* **29** 74704
[19] Sobac B and Brutin D 2012 *Phys. Fluids* **24** 032103
[20] Brutin D, Sobac B, Rigolle F and Niliot C L 2011 *Exp. Therm. Fluid Sci.* **35** 521
[21] Zhou B, Zhu P, Duan L and Kang Q 2013 *Mechanics in Engineering* **35** 39 (in Chinese)